

# Search for the correction term to the Fermi's golden rule in positron annihilation

R. Ushioda<sup>1,\*</sup>, O. Jinnouchi<sup>1</sup>, K. Ishikawa<sup>2,3</sup>, and T. Sloan<sup>4</sup>

<sup>1</sup>*Department of Physics, Faculty of Science, Tokyo Institute of Technology, Tokyo 152-8551, Japan*

<sup>2</sup>*Department of Physics, Faculty of Science, Hokkaido University, Sapporo 060-0810, Japan*

<sup>3</sup>*Research and Education Center for Natural Sciences, Keio University, Kanagawa 223-8521, Japan*

<sup>4</sup>*Department of Physics, University of Lancaster, Lancaster LA1 4YB, United Kingdom*

\*E-mail: ushioda@hep.phys.titech.ac.jp

In the positron-electron annihilation process, finite deviations from the standard calculation based on the Fermi's Golden rule are suggested in recent theoretical work. This paper describes an experimental test of the predictions of this theoretical work by searching for events with two photons from positron annihilation of energy larger than the electron rest mass (511 keV). The positrons came from a  $^{22}\text{Na}$  source, tagging the third photon from the spontaneous emission of  $^{22}\text{Ne}^*$  de-excitation to suppress backgrounds. Using the collected sample of  $1.06 \times 10^7$  positron-electron annihilations, triple coincidence photon events in the signal enhanced energy regions are examined. The observed number of events in two signal regions,  $N_{\text{obs}}^{\text{SR1}} = 0$  and  $N_{\text{obs}}^{\text{SR2}} = 0$  are, within a current precision, consistent with the expected number of events,  $N_{\text{exp}}^{\text{SR1}} = 0.86 \pm 0.08(\text{stat.})^{+1.85}_{-0.81}(\text{syst.})$  and  $N_{\text{exp}}^{\text{SR2}} = 0.37 \pm 0.05(\text{stat.})^{+0.80}_{-0.29}(\text{syst.})$  from Fermi's golden rule respectively. Based on the  $P^{(d)}$  modeling, the 90% CL upper limit on the photon wave packet size is obtained.

Subject Index      xxxx, xxx

## 1. Introduction

The process of positron annihilation to two photons is a simple system and their detection is suitable for a precision test of quantum electro-dynamics (QED). A transition probability of the quantum process,  $P(T)$ , at time  $T$  is formulated by the Fermi's golden rule with a certain approximation [1, 2], i.e.  $P(T) = \Gamma T$ , where  $\Gamma$  is the average transition rate. A problem of this approximation has been pointed out by several theoretical considerations, and it is suggested that an additive constant correction term,  $P^{(d)}$ , is required in the formulation as in Eq. (1) [3].

$$P(T) = \Gamma T + P^{(d)} \quad (1)$$

The correction term to the golden rule is often dismissed or ignored due to its unusual property underived from the golden rule, and thus far it has been a good approximation when it is compared to the experimental quantities in the golden rule. This holds true for a slow process where  $T$  is large, but it is concerned to be insufficient for rapidly changing processes where the relatively sizable effect for the correction term can be expected [4]. Although the processes based on the correction term,  $P^{(d)}$ , can show a unique signature of its non-conserving nature of the kinetic energies, experimental confirmation of the effect

has not been hitherto seriously pursued mainly due to its predicted broad spectrum, which would lie under the backgrounds, preventing its manifestation.

In a recent article [5], it is proposed that the two photon process of the position annihilation could manifest a sizable correction. In the same article, the feasibility of an experiment using a simple setup is discussed. As suggested in the article, a setup based on the  $^{22}\text{Na}$  radioactive source surrounded by the  $\gamma$ -ray detectors, e.g. NaI(Tl) scintillation detectors, is an ideal platform for verifying such effect. From the process,  $^{22}\text{Na} \rightarrow ^{22}\text{Ne}^* + e^+ + \nu, e^+ + (e^-) \rightarrow \gamma_1 + \gamma_2$ , two photons with the same energies in opposite directions are expected. Here,  $(e^-)$  is the electrons resident within the materials near the source. In Fermi's golden rule, the energies of the two photons are the electron rest mass, i.e.  $E_{\gamma_1} = E_{\gamma_2} = 511 \text{ keV}$ , while with correction term,  $P^{(d)}$ , it can be deviate from 511 keV as illustrated in Fig. 1. In experiment,

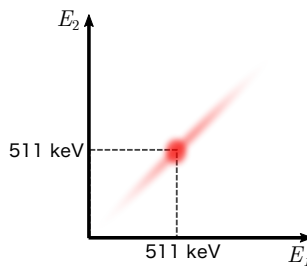


**Fig. 1** Expected correlation between two photon energies with  $P^{(d)}$ . A filled circle at 511 keV represents the events from Fermi's golden rule.

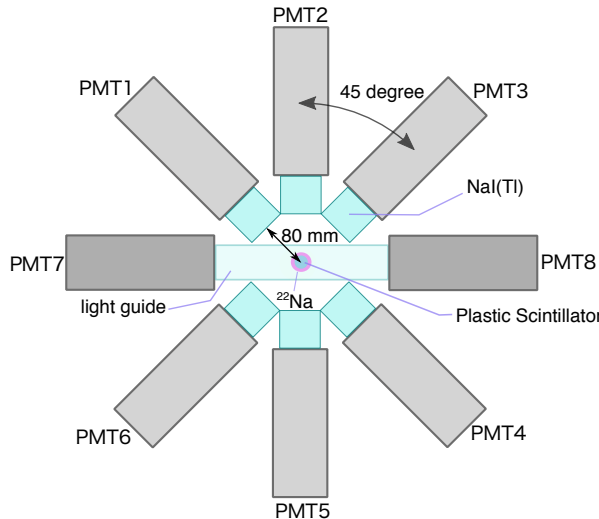
low energy range ( $E_{\gamma_1} = E_{\gamma_2} < 511 \text{ keV}$ ) suffers a huge backgrounds produced via Compton scattering of the 511 keV photons. Conversely, the high energy range ( $E_{\gamma_1} = E_{\gamma_2} > 511 \text{ keV}$ ), is free from such backgrounds. Exception is those from double hit pileup events discussed in Sec. 3. Events requiring two photons in opposite direction is named *2-coincidence events*, and it is not enough to suppress the double hit pileup backgrounds. However, in the process of  $^{22}\text{Na}$  decays, the third photon ( $E_{\gamma_0} = 1274.5 \text{ keV}$ ) is emitted almost simultaneously to the positron annihilation via the de-excitation process of  $^{22}\text{Ne}^*$  nucleus. Tagging of this third photon is effective in significantly suppressing the double hit backgrounds. In this paper, the events requiring three photons, one with 1274.5 keV and the other two being detected in back-to-back configuration in higher energy range, is named *3-coincidence events*, and is treated as the signal events.

This paper is organized as follows. In section 2, the setup of the experiment is described. In Section 3, the models and the methodologies of the background estimation is explained. Section 4, describes the data analysis. Section 5 summarizes the results, and the results are interpreted in Section 6. Section 7 concludes this new measurement.

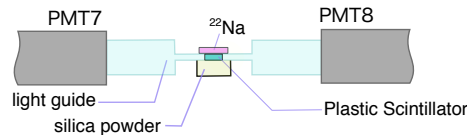
## 2. Experimental Setup

Figure 2 is the top view of the experimental setup. The  $^{22}\text{Na}$  radioactive source (Japan isotope center, 3 mm diameter aperture, 25 kBq) [6] is placed at the center, which is surrounded by the six cylindrical shaped NaI(Tl) scintillators (see later text for detail), named as PMT1 to 6. As in the figure, three pairs are made in back-to-back configuration with respect to the source, between them are separations of 45 degrees each. Scintillators face to the center

of the setup, and the distance between their surface and the center is 80 mm. In the centre is placed a  $^{22}\text{Na}$  radioactive source with the positron tagging system as shown in Fig. 3. A thin plastic scintillator plate (Saint-Goban,  $\phi 7.5\text{mm} \times t 0.1\text{mm}$ , BC-408, Polybinytoluene 1.023 g/cc [7]) is placed beneath the  $^{22}\text{Na}$  source, following is the small container filled with the  $\text{SiO}_2$  powder (NIPPON AEROSIL, R812 (density:  $\sim 60\text{ mg/cm}^3$ , Specific surface area:  $230 - 290\text{ m}^2/\text{g}$ ) [8]). Positrons ejected from the source scintillate in the thin plate scintillator. The scintillation light propagates through the thin lightguides on both sides (CI Industry Co. Ltd. [9],  $t 2\text{ mm} \times 30\text{ mm} \times 39\text{ mm}$ ) and the second lightguides ( $\phi 38\text{ mm} \times t 109.7\text{ mm}$ ), then readout by two Photomultipliers (Hamamatsu H6410). These PMTs are named PMT 7 and 8, and the coincidences of these are considered as the positron signals and used as triggers. Positrons are trapped inside aerogel pores of the silica powder and annihilate into two photons. In order to reduce the contribution from positronium formation, the silica powder container is filled with air. This positron signal timing is used to suppress the accidental background by requiring two detections, one from the combination of the  $\gamma$ -ray detections and one from the positron signals. Additionally, requirement of positron signal in plastic scintillator can constrain the positron annihilation position to be inside the  $\text{SiO}_2$  powder case.



**Fig. 2** Schematic illustration of the experimental setup top view.



**Fig. 3** Schematic illustration of the positron source setup side view.

For the  $\gamma$ -ray detection,  $6 \times \text{NaI(Tl)}$  scintillators (OHYO KOKEN, 8B8 ( $\phi 50.8\text{ mm} \times t 50.8\text{ mm}$ ) [10]) are used. The NaI crystal is sealed in aluminum housing (4.0 mm thick

---

in front, 2.8 mm thick on the sides). Scintillation light is readout by PMTs (Hamamatsu, H6410, H7195, H1161-50, [11]).

A CAMAC system (controller TOYO Corporation CC/NET [12]) interfaced to a PC was used for the data acquisition. The analogue signals were handled with the NIM standard modules, for the digitization, timing adjustment, and taking coincidence. As the energy deposit of positron on the thin plastic scintillator is small, the outputs of PMT 7 and 8 are amplified with FastAmp (Kaizuworks Corporation, 2104[13]). They are digitized with low threshold, and timing coincidence of PMT 7 and 8 is required to mitigate the fake signals from the noise. One outputs from each PMT 1 to 6 are fed into discriminator module, and the signal timings are defined by the digitized outputs of them. A hardware coincidence of the positron signal and at least one hit out of six PMTs for the photons (PMT 1-6), is used as a trigger for the data taking. Time difference,  $\delta t_i$ , between positron signal and each photon detector ( $i = 1 - 6$ ) is measured with the Time to Digital Converter (TDC, Technoland Corporation, C-TS103, 125 ps resolution [14]). Other outputs from each PMT 1 to 6 (each PMT has two anode outputs) are used to measure the energy depositions inside NaI(Tl). In order to measure the energy deposition, these outputs are subdivided into two lines, and are fed to a charge sensitive Analogue to Digital Converter (ADC, Hoshin Electronics Co., LTD., C009 [15]) with different gate widths to mitigate the pile-up events. Hereafter they are called  $\text{ADC}_{\text{wide}}$  (gate width 1.2  $\mu\text{s}$ ) and  $\text{ADC}_{\text{narrow}}$  (gate width 100 ns).

### 3. Backgrounds

Although there is no intrinsic background source for this experiment, where two photons with large energies radiated in back-to-back directions, there are several potential sources which mimic the signal.

One such background is the environmental radiations from walls of the experimental room. In order to reduce this, a coincidence in timing between the positron emission and the photon detections is required. Accidental coincidence rate,  $R_{\text{acc}}$ , is expected to be in the form,  $R_{\text{acc}} = R_{e^+} \times R_{\gamma} (h_{e^+} + h_{\gamma} - 2h_{\text{coin}})$ , where  $R_{e^+}$  is the positron detection rate ( $\sim 100 \text{ Hz}$ ),  $R_{\gamma}$  is the environmental radiation detection rate ( $\sim 0.17 \text{ Hz}$ ),  $h_{e^+}$  is the pulse width of the positron signal ( $\sim 100 \text{ ns}$ ),  $h_{\gamma}$  is the pulse width of the photon signal ( $\sim 100 \text{ ns}$ ), and  $h_{\text{coin}}$  is the minimum time width required for the coincidence ( $\sim 10 \text{ ns}$ ). During the measured time (550 hours), 5 events are expected from the environmental background which concentrate in photon energies below 511 keV. Hence the environmental radiations are safely ignored.

Main background events stem from the double hits pileup, where the data acquisition is incapable to separate two sequential  $^{22}\text{Na}$  decays due to the finite time window of the coincidence module. These pileup events can be suppressed by the comparisons of the two ADC measurements for the photon energies. However it can only reduce the pileup event rate down to  $O(10^{-4})$ , therefore the simulation based estimation is vital.

Figure 4 shows several event configurations. Figure 4(a) represents the nominal event case where 511 keV photons from annihilations are detected in opposite side detectors. Figure 4(b) is the double hit background where two pairs of 511 keV photons are detected, i.e. 1022 keV energies in back-to-back detectors. Figure 4(c) is another type of double hit background. In this case, two 1275 keV photons from different decays are detected in opposite detector pair by accident.

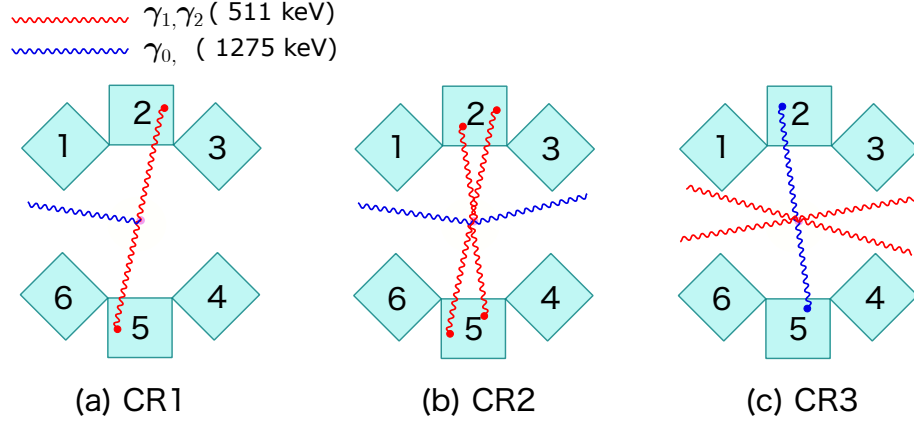


**Fig. 4** 2 coincidence event types considered in this analysis. See text for description for each drawing.

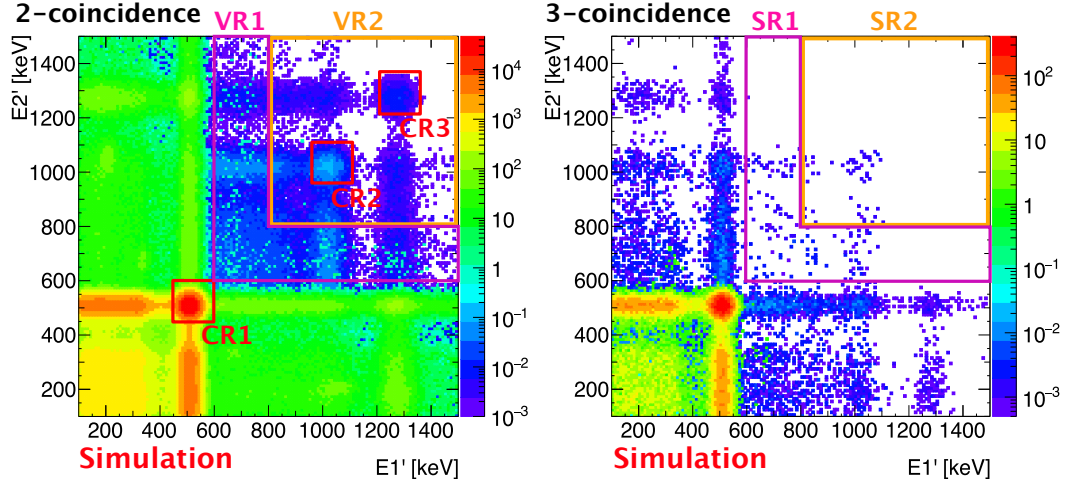


**Fig. 5**  $E'_2$  vs.  $E'_1$  distributions estimated with the simulations.

In order to estimate the double hit background events in 2- or 3-coincidence events, a detector simulation based on the Geant4 toolkit[16] has been setup. The detector components and materials in Fig. 2 and Fig. 3 are reproduced in the simulation. In single hit events, two 511 keV back-to-back annihilation photons, and a 1275 keV photon are simulated, while in double hit events two pairs of back-to-back 511 keV photons and two 1275 keV photons are simulated. In these simulations, 1275 keV photons are emitted isotropically from the  $^{22}\text{Na}$  source, and the positron annihilations are generated inside the silica powder container.

$2 \times 10^8$  simulation events are generated in both types of events. In order to reproduce the experimental data, single hit events and double hit events are summed with the proper weights. The weights are estimated by using the experimental data as explained in Sec.4.

In this experiment, the *2-coincidence* detection is defined as follows. 2-coincidence : “photons are detected in more than or equal to 2 detectors and only one pair of them are in

---

**Table 1** Definitions of the CR, SR and VR regions (see Fig. 5 for a pictorial illustration of the different named regions.). The remaining number of events out of  $2 \times 10^8$  simulated event samples, i.e. single hit and double hit events, after the energy cuts, and  $c_{ij}$  correction (see Sec. 4 for definition) are shown in 4th and 5th columns.

regions	condition	energy cut	$N_{\{\text{regions}\},\text{single}}^{\text{simul}}$	$N_{\{\text{regions}\},\text{double}}^{\text{simul}}$
CR1	2-coin.	$450 \text{ keV} \leq E'_1, E'_2 \leq 600 \text{ keV}$	$1.52 \times 10^6$	$2.88 \times 10^6$
CR2	2-coin.	$961 \text{ keV} \leq E'_1, E'_2 \leq 1111 \text{ keV}$	0	$3.50 \times 10^3$
CR3	2-coin.	$1213.5 \text{ keV} \leq E'_1, E'_2 \leq 1363.5 \text{ keV}$	0	$3.02 \times 10^3$
VR1	2-coin	when $E'_i \leq E'_j$ , $600 \text{ keV} \leq E'_i \leq 800 \text{ keV}$ , $600 \text{ keV} \leq E'_i \leq 1500 \text{ keV}$	$2.15 \times 10^2$	$2.84 \times 10^4$
VR2	2-coin	$800 \text{ keV} \leq E'_1, E'_2 \leq 1500 \text{ keV}$ (excluding CR2, CR3)	2.1	$1.59 \times 10^4$
SR1	3-coin.	when $E'_i \leq E'_j$ , $600 \text{ keV} \leq E'_i \leq 800 \text{ keV}$ , $600 \text{ keV} \leq E'_i \leq 1500 \text{ keV}$	0	$2.40 \times 10^2$
SR2	3-coin.	$800 \text{ keV} \leq E'_1, E'_2 \leq 1500 \text{ keV}$	0	$1.07 \times 10^2$

opposite direction, i.e. excluding the events with two or more opposite direction pairs.” Similarly the *3-coincidence* detection is defined as follows. “3-coincidence : photons are detected in one opposite direction pair detectors, and in an additional detector. The energy deposit in additional detector,  $E'_3$ , should be,  $1200 \text{ keV} \leq E'_3 \leq 1390 \text{ keV}$ . As in the case for the 2-coincidence, the events having two or more opposite direction pairs are excluded.” Requirement on  $E'_3$  strongly suppresses the backgrounds of type (c) in Fig. 4 where two 1275 keV photons accidentally hit the opposite side detectors.

In these coincidence events, energy depositions in the opposite direction pair are named as  $E'_1$  and  $E'_2$ , where  $E'_1$  is measured with one of PMT-1, 2 and 3. Similarly,  $E'_2$  is the one from PMT-4,5 and 6. In the 2-dimensional phase space of  $E'_1$  and  $E'_2$ , three control regions (CRs) are defined. These CRs abound with background in 2 coincident events, and they are used to normalize the distributions from simulation to the measured data. Also defined are the two signal regions (SRs), where large signal to background ratio is expected, and two validation regions (VRs) which are used to check the validity of background estimation at the region close to SRs. They are defined in Table. 1. The definition of these regions can be graphically confirmed in Fig. 5. CR1 is dominated by those events in which both 511 keV photons are photoelectrically absorbed (Fig. 4(a)). The number of events in CR1,  $N_{\text{CR1}}^{\text{data}}$ , is used to normalize the simulation to the observed data. CR2 corresponds to the double hit events in which two pairs of 511 keV photons are all photoelectrically absorbed (Fig. 4(b)). Number of events in CR2,  $N_{\text{CR2}}^{\text{data}}$ , is used to estimate the amount of pileup. On the other hand, CR3 corresponds to the double hit events in which two 1275 keV photons from different events are photoelectrically absorbed (Fig. 4(c)). Number of events in CR3,  $N_{\text{CR3}}^{\text{data}}$ , is used to estimate the amount of accidental background. VRs suffer from less backgrounds, but they still contain good amount of backgrounds. These are mainly from those events where one, or both of two photons in CR2 or CR3 are Compton scattered. These regions can potentially contain contamination from the signal events but are expected to be largely dominated by the background, thus it is considered to be safe to use these as VRs. SR1 and SR2 are the

---

same as VR1 and VR2 respectively except they require 3-coincidence, and backgrounds are largely suppressed.

#### 4. Data Analysis

$1.06 \times 10^7$  events were recorded in 550 hours, which corresponds to the average data acquisition rate of 5.4 Hz. Data were taken in 13 runs.

The energy scale of the detectors were calibrated *in situ* using the photo-electric absorption peaks (511 keV, 1275 keV) from the  $^{22}\text{Na}$  source for each run. A linear function is used for the calibration. The TDC is a clock counter type module, and the linearity of  $\pm 500$  ps is guaranteed. Hence no calibration runs were taken for TDC.

In order to retain adequate quality of data, the following preselections are applied. Since the signal is prompt positron annihilation, the time difference between the trigger (positron annihilation) and the photon detection, is constant.  $|\delta t| < 1$  nsec around the mean timing is required. The slewing effect is confirmed to be very small for relevant energy range ( $> 200$  keV), hence the slewing correction for the photon detection, i.e. energy dependent timing correction, is not applied in this analysis.

The standard deviation of the time resolution in each photon detector is 1.2 nsec, and the time difference between photon detections within  $\pm 6$  nsec are used as the coincidence events. As described in Sec. 2, for each photon detection, two ADC measurements with different gate widths are utilized to suppress the pileup events. For the signal regions ( $E^{(i)} > 600$  keV,  $i=1-6$ ), a cut on event  $E_{\text{wide}}^{(i)} - E_{\text{narrow}}^{(i)} < 100$  keV is applied. After the preselections, the event selections for control and validation regions are applied.

Table 2 summarizes the number of remaining events after the event selection for control regions as defined in Table 1. Mis-modeling of the simulation is evaluated by the comparison of data and simulated distributions in the region next to CR1 ( $450 \text{ keV} \leq E'_i \leq 600 \text{ keV}$ ,  $600 \text{ keV} \leq E'_j \leq 1500 \text{ keV}$ ,  $i, j = 1, 2, i \neq j$ ). The correction factors are extracted from this comparison, and are applied to the simulated events to compensate the differences. The regions ( $E'_1, E'_2 > 600$  keV) are binned in 2D-matrix in every 100 keV, and each region is corrected by the correction factor,  $c_{ij} = c_i^{(1)} \times c_j^{(2)}$ , where  $c_i^{(1)}, c_j^{(2)}$  turned out to be values between 0.7 to 1.3 depending on the energy.  $c_i^{(1)}, c_j^{(2)} (i, j = 1, 2, 3, \dots)$  are the factors for  $E'_1, E'_2$  respectively.

Using these experimentally obtained numbers, the accidental background rate and the pileup event rate are evaluated as follows. The accidental backgrounds originate from the double hit events and appear in CR3 where two 1275 keV photons are accidentally detected in opposite side detectors in the time window of this experiment. The accidental background event rate i.e. the ratio of double hit events to single hit events, named  $\alpha$ , is determined from the equation,  $N_{\text{CR3}}^{\text{data}}/N_{\text{CR1}}^{\text{data}} = (N_{\text{CR3,single}}^{\text{simul}} + \alpha N_{\text{CR3,double}}^{\text{simul}})/(N_{\text{CR1,single}}^{\text{simul}} + \alpha N_{\text{CR1,double}}^{\text{simul}})$ .  $\alpha$  is estimated to be  $\alpha = (3.35^{+4.43}_{-2.16}) \times 10^{-4}$ . The estimated number of events in CR1, CR2 and CR3 after taking  $\alpha$  into account, are  $N_{\text{CR1},\alpha}^{\text{estim}} = 1.52 \times 10^6$ ,  $N_{\text{CR2},\alpha}^{\text{estim}} = 1.17$ , and  $N_{\text{CR3},\alpha}^{\text{estim}} = 1.01$  respectively. Since the rejection power for pileup backgrounds after the timing coincidence is weaker than for accidental background, more pileup events are expected in CR2 and in associated lower energy range. In order to estimate this amount, another type of simulation sample, called *semi-double event*, containing two pairs of 511 keV photons and one 1275 keV photon per event, are generated, aiming to simulate the pileup events which appear in CR2 and not

**Table 2** The number of events in 2-coincidence control regions after the selections.

regions	name	number of events
CR1	$N_{\text{CR1}}^{\text{data}}$	$3.01 \times 10^6$
CR2	$N_{\text{CR2}}^{\text{data}}$	14
CR3	$N_{\text{CR3}}^{\text{data}}$	2

**Table 3** The normalized simulated number of events in various regions. The subscripts ' $\alpha\beta$ ' represents the corrections made for parameters,  $\alpha$  and  $\beta$ .

regions	$N_{\{\text{regions}\},\alpha\beta}^{\text{simul}}$
CR1	$1.53 \times 10^6$
VR1	$2.56 \times 10^2$
VR2	$1.53 \times 10^1$
SR1	$2.79 \times 10^{-1}$
SR2	$1.21 \times 10^{-1}$

in CR3. The remaining number of events in CR1 and CR2, out of generated  $2 \times 10^8$  semi-double events,  $N_{\text{CR1,semi}}^{\text{simul}}$ ,  $N_{\text{CR2,semi}}^{\text{simul}}$ , are found to be,  $N_{\text{CR1,semi}}^{\text{simul}} = 2.92 \times 10^6$ ,  $N_{\text{CR2,semi}}^{\text{simul}} = 2.85 \times 10^3$ . The ratio of pileup events to accidental events in CR2,  $\beta$ , is determined from the equation,  $N_{\text{CR2}}^{\text{data}}/N_{\text{CR1}}^{\text{data}} = (N_{\text{CR2},\alpha}^{\text{estim}} + \beta N_{\text{CR2,semi}}^{\text{simul}})/(N_{\text{CR1},\alpha}^{\text{estim}} + \beta N_{\text{CR1,semi}}^{\text{simul}})$ , and found to be  $\beta = (2.08_{-1.93}^{+2.57}) \times 10^{-3}$ . Based on the parameters,  $\alpha$  and  $\beta$ , the numbers of simulated

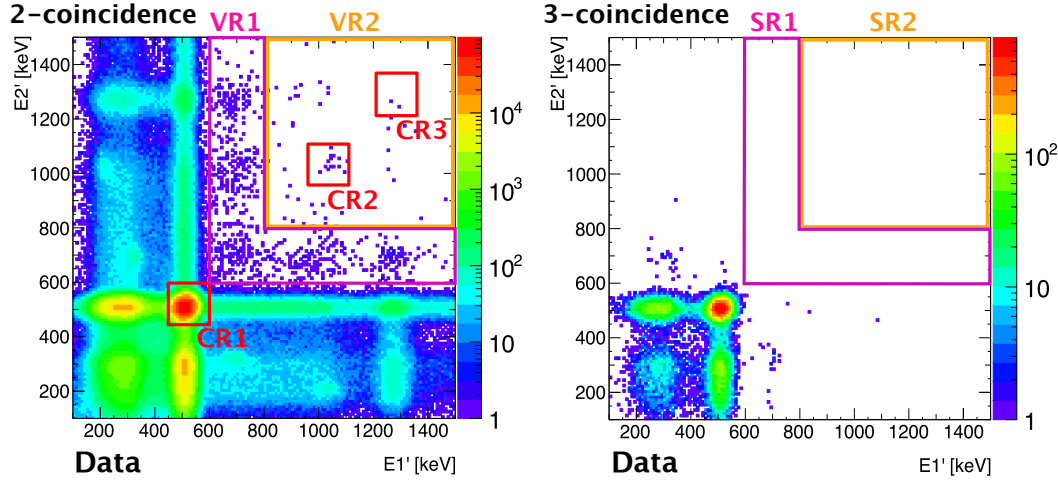


**Fig. 6**  $E'_2$  vs.  $E'_1$  distributions obtained with data.

events in various regions are normalized. Obtained values are summarized in Table 3.

The detector components are aligned, and the precision of the geometrical alignments are expected to be within  $\pm 1$  mm. The systematics errors related to following items are estimated. The distance between the photon detectors and the center of the setup, the tilt of the setup, i.e. the angular deviation of the detectors from the setup design, the actual

---

**Table 4** The number of events in signals regions. The second column is the observed number of events in data, and the third column is the expected number of events from background estimation.

regions	$N_{\text{SR}i}^{\text{data}}(i = 1, 2)$	$N_{\text{SR}i}^{\text{exp, corre}}(i = 1, 2)$
SR1	0	$0.86 \pm 0.08(\text{stat.})^{+1.85}_{-0.81}(\text{syst.})$
SR2	0	$0.37 \pm 0.05(\text{stat.})^{+0.80}_{-0.29}(\text{syst.})$

location of the annihilations inside the powder case, etc. All these are checked using the simulation, and confirmed to have negligible contributions to the result.

## 5. Results

VR1 is used to check the validity of the background estimations. In VR1, number of events in data is found to be consistently higher than the estimation (mean factor 1.56), hence the constant correction is applied on the estimation (VR1 correction) to remove this difference. A remained bin by bin fluctuation is approximately 40%, which is counted as the systematic errors. After the VR1 correction, VR2 is used for the final validity check of the method. 46 events are observed in data ( $N_{\text{VR1}}^{\text{data}}$ ), where  $N_{\text{VR1}}^{\text{estim, corre}} = 47.0^{+8.6}_{-4.5}(\text{stat.})^{+90.9}_{-27.5}(\text{syst.})$  events are expected from the background estimation. A superscript 'corre' represents the corrections made for parameters  $\alpha, \beta$ , and the factor 1.56.

The signal regions are unblinded after this confirmation. Figure 6 is the observed  $E'_2$  vs.  $E'_1$  distributions of the 2-coincidence (left) and 3-coincidence (right) events. Table 4 summarizes the results in two SRs. The expected values in two SRs are obtained as,  $N_{\text{SR}i}^{\text{exp, corre}} = N_{\text{SR}i, \alpha\beta}^{\text{simul}} \times (N_{\text{CR}1}^{\text{data}}/N_{\text{CR}1, \alpha\beta}^{\text{simul}}) \times 1.56$  ( $i = 1, 2$ ).

0 events are observed in both signal regions, where  $N_{\text{SR}1}^{\text{exp, corre}} = 0.86 \pm 0.08(\text{stat.})^{+1.85}_{-0.81}(\text{syst.})$  and  $N_{\text{SR}2}^{\text{exp, corre}} = 0.37 \pm 0.05(\text{stat.})^{+0.80}_{-0.29}(\text{syst.})$  background events are predicted in SR1 and SR2, respectively. With the current experimental precision, the results are consistent with the background prediction expected from the Fermi's golden rule. Relatively large systematic errors stem from the propagated uncertainties of the  $\alpha, \beta$  parameters, which originated from the limited statistics in  $N_{\text{CR}2}^{\text{data}}$  and  $N_{\text{CR}3}^{\text{data}}$ .

## 6. Interpretation

In the article [5], the relative size of  $P^{(d)}$  correction term for the positron annihilation is predicted as a function of the photon wave packet size,  $\sigma_\gamma$ , for power-law and Gaussian wave functions. Figure 1 of the article [5], illustrates the expected ratio of events from  $P^{(d)}$  per positron in SR2. Since 0 events were observed in SR2, 90% CL upper limit,  $N_{\text{obs}}^{\text{SR}2, 90\text{CL}}$ , is 2.30 events [17]. The efficiencies of detecting photons in the NaI(Tl) scintillator with 800 keV threshold,  $\varepsilon_\gamma$ , are estimated with simulation. It is gradually increasing as a function of the incident photon energy, e.g. for the photon energies of 1 MeV and 1.5 MeV, they are estimated to be 28% and 38% respectively. Upper limit of the  $P^{(d)}$  per positron in SR2 is,  $P_{\text{SR}2, 90\text{CL}}^{(d)} = (N_{\text{obs}}^{\text{SR}2, 90\text{CL}} - 0.37)/N_{511\text{keV}}^{\text{3-coincidence}}/\varepsilon_\gamma^2$ , where  $N_{511\text{keV}}^{\text{3-coincidence}}$  is the number of events of the positron annihilation in 3 coincidence events observed around the photo electric peak in both  $E'_1$  and  $E'_2$ , and is observed to be 23085. Using the mean value,  $\varepsilon_\gamma = 33 \pm 5\%$ ,  $P_{\text{SR}2, 90\text{CL}}^{(d)} = (7.68 \pm 0.20(\text{stat.})^{+3.94}_{-2.67}(\text{syst.})) \times 10^{-4}$  is obtained, whose central value corresponds to  $\sigma_\gamma = 2.4 \times 10^{-20} \text{ m}^2$  with the power-law wave function dominant model [5].

---

## 7. Conclusion

In investigating the correction term of the Fermi's golden rule, the experimental test to search for the positron annihilation events with high energy two photons is carried out. 0 events are observed in two signal regions, where  $0.86 \pm 0.08(\text{stat.})^{+1.85}_{-0.81}(\text{syst.})$ ,  $0.37 \pm 0.05(\text{stat.})^{+0.80}_{-0.29}(\text{syst.})$  are expected respectively. The result in the second signal region is interpreted with the  $P^{(d)}$  model, yielding 90% CL upper limit on the photon wave packet size,  $\sigma_\gamma = 2.4 \times 10^{-20} \text{ m}^2$  in the power-law wave function dominant model. This is the first experiment to look into this correction term using the positron annihilation.

## Acknowledgment

The authors thank A. Kubota, T. Matsuzaki for useful discussions.

## References

- [1] P.A.M. Dirac, Pro. R. Soc. Lond. A **114**, 243, (1927).
- [2] L.I. Schilff, Quantum Mechanics (McGRAW-Hill book, company, Inc. New York), (1955).
- [3] K. Ishikawa and Y. Tobita, Prog. Theor. Exp. Phys. **2013**, no. 7, 073B02, (2013).
- [4] K. Ishikawa and K. Oda, Prog. Theor. Exp. Phys. **2018** no. 12, 123B01, (2018).
- [5] K. Ishikawa, O. Jinnouchi, A. Kubota, T. Sloan, T.H. Tatsuishi, and R. Ushioda, Prog. Theor. Exp. Phys. **2019**, no. 3, 033B02, (2019).
- [6] Japan Radioisotope Association <https://www.jriias.or.jp/e/index.html>
- [7] Saint-Gobain Crystals, <https://www.crystals.saint-gobain.com>
- [8] NIPPON AEROSIL CO., LTD., <https://www.aerosil.com/product/aerosil/en>
- [9] Japan CI Industry Co. Ltd., <http://www.cikogyo.co.jp>
- [10] OHYO KOKEN KOGYO CO., LTD., <http://www.oken.co.jp/en/index.html>
- [11] Hamamatsu Photonics K. K., <https://www.hamamatsu.com/jp/en/index.html>
- [12] TOYO Corporation, <https://www.toyo.co.jp/english/>
- [13] Kaizuworks Corporation, <http://www.kaizuworks.co.jp/index-English.html>
- [14] Techno Corporation, <http://www.tcnland.co.jp/?lang=en>
- [15] Hoshin Electronics Co., LTD., <https://www.kagaku.com/hoshin/english.html>
- [16] Geant4 Collaboration, Nucl. Instrum. Meth. A **506**, 250, (2003).; Geant4 Collaboration, IEEE Trans. Nucl. Sci. **53** No. 1, 270, (2006).; Geant4 Collaboration, Nucl. Instrum. Meth. A **835**, 186, (2016).
- [17] M. Tanabashi et al. (Particle Data Group), Phys. Rev. D **98**, 030001 (2018).